

replaced with a mixture of TEOS and *bis*-TMSEN. Thus, mixtures of 30.3 *X* mmol of *bis*-TMSEN and 30.3 (1-*X*) mmol TEOS, where *X* = 0.02 and 0.05, were used for the synthesis instead of pure TEOS. The materials resulting from these syntheses were designated HMS-ENIS-2 % and HMS-ENIS-5 %, respectively.

**Characterization:** Powder X-ray diffraction patterns were measured on a Rigaku Rotaflex diffractometer equipped with a rotating anode and using Cu K $\alpha$  radiation (Ontario Geoscience Laboratories, Sudbury, Ontario, Canada). N<sub>2</sub> adsorption isotherms of the adsorbents were measured at -196 °C on a Micromeritics ASAP 2010 instrument. Prior to measurement, all samples were outgassed at 110 °C at 10<sup>-6</sup> mm Hg. BET surface areas were measured from the linear part of the BET plot (0.05 < *P/P*<sub>0</sub> < 0.25). Mesopore volumes (*V*<sub>mp</sub>) were assumed to be equal to the liquid volume of adsorbed nitrogen at *P/P*<sub>0</sub> = 0.7. Pore size distributions were calculated using the Broekhoff-deBoer (BdB) method [23].

**Metal Ion Adsorption:** 20 mg portions of each mesostructure were stirred for 12 h with 10 mL of buffered (pH 5.0) M(NO<sub>3</sub>)<sub>2</sub> solutions ([M<sup>2+</sup>] = 1.6 × 10<sup>-5</sup> to 1.6 × 10<sup>-4</sup> M, in phthalate buffer), where M = Cu, Ni, or Zn. The mixtures were then filtered and the residual metal ion concentrations in the filtrates analyzed by flame atomic absorption spectroscopy (AAS). The adsorption capacities of each adsorbent for Cu<sup>2+</sup>, Ni<sup>2+</sup>, and Zn<sup>2+</sup> were then determined from the concentration difference measured between the filtrates and the initial metal ion solutions. The distribution coefficients (*K*<sub>d</sub>) for each adsorbent-metal system were also determined using the equation [8-11]:

$$K_d = (C_i - C_f) V_{sol} / (C_f m_{ads}) \quad (1)$$

where *C*<sub>i</sub> is the initial metal ion concentration of the solution, *C*<sub>f</sub> is the metal ion concentrations after adsorption, *V*<sub>sol</sub> is the volume of the solution [mL], and *m*<sub>ads</sub> is the amount of adsorbent used [g].

**Adsorbent Regeneration:** The Cu<sup>2+</sup>-loaded HMS-ENIS adsorbents (0.1 g) were stirred in 20 mL of 1 M HNO<sub>3</sub> for 30 min, then recovered by filtration. The adsorbents were then slurried in 50 mL of deionized water and titrated to neutral pH (7.0) with 1 M NaOH. The materials were recovered by filtration and air-dried. The metal ion adsorption properties of the regenerated adsorbents were then evaluated following the previously described method.

Received: February 25, 2002

## Self-Assembled Nanowire Networks by Deposition of Copper onto Layered-Crystal Surfaces\*\*

By Rainer Adelung,\* Frank Ernst, Adina Scott, Massood Tabib-Azar, Lutz Kipp, Michael Skibowski, Stefan Hollensteiner, Erdmann Spiecker, Wolfgang Jäger, Stefan Gunst, Andreas Klein, Wolfram Jägermann, Vladimir Zaporozhchenko, and Franz Faupel

We report on the discovery that deposition of copper onto layered crystals (VSe<sub>2</sub>) induces the formation of self-assembled nanowire networks. While a similar phenomenon was discovered recently<sup>[1]</sup> when depositing Rb onto layered crystals, the Cu-induced nanostructures are of much higher practical use because they are stable under ambient conditions. Moreover, Cu deposition induces the formation of nanotunnels on the layered-crystal surface.

In this publication, we will first explain how Cu-induced nanostructures are grown. Second, we present preliminary results on their microscopic structure and properties, obtained by employing various techniques of microcharacterization. Third, we propose a theory about their formation mechanism. Finally, we demonstrate their application potential in nanotechnology.

Immediately after the Cu evaporation was performed, the specimens were transferred to a neighboring ultra-high vacuum (UHV) chamber (without leaving the UHV) and studied by scanning tunneling microscopy (STM). Figure 1a shows a typical result of this experiment: nanoscopic wires form on the substrate surface, and these wires arrange themselves in a

- [1] C. T. Kresge, M. E. Leonowicz, W. J. Roth, J. C. Vartuli, J. S. Beck, *Nature* **1992**, 359, 710.
- [2] A. Sayari, S. Hamoudi, *Chem. Mater.* **2001**, 13, 3151.
- [3] L. Mercier, T. J. Pinnavaia, *Adv. Mater.* **1997**, 9, 500.
- [4] X. Feng, G. E. Fryxell, L.-Q. Wang, A. Y. Kim, J. Liu, K. M. Kemner, *Science* **1997**, 276, 923.
- [5] L. Mercier, T. J. Pinnavaia, *Environ. Sci. Technol.* **1998**, 32, 2749.
- [6] J. Brown, L. Mercier, T. J. Pinnavaia, *Chem. Commun.* **1999**, 69.
- [7] J. Brown, R. Richer, L. Mercier, *Microporous Mesoporous Mater.* **2000**, 37, 41.
- [8] S. Dai, M. C. Burleigh, Y. Shin, C. C. Morrow, C. E. Barnes, Z. Xue, *Angew. Chem. Int. Ed.* **1999**, 38, 1235.
- [9] S. Dai, Y. Shin, Y. Ju, M. C. Burleigh, J.-S. Lin, C. E. Barnes, Z. Xue, *Adv. Mater.* **1999**, 11, 1226.
- [10] S. Dai, M. C. Burleigh, Y. H. Ju, H. J. Gao, J. S. Lin, S. J. Pennycook, C. E. Barnes, Z. L. Xue, *J. Am. Chem. Soc.* **2000**, 122, 992.
- [11] M. C. Burleigh, S. Dai, E. W. Hagaman, J. S. Lin, *Chem. Mater.* **2001**, 13, 2537.
- [12] S. Inagaki, S. Guan, Y. Fukushima, T. Ohsuna, O. Terasaki, *J. Am. Chem. Soc.* **1999**, 121, 9611.
- [13] B. J. Melde, B. T. Holland, C. F. Blanford, A. Stein, *Chem. Mater.* **1999**, 11, 3302.
- [14] T. Asefa, M. J. MacLachlan, N. Coombs, G. A. Ozin, *Nature* **1999**, 402, 867.
- [15] C. Yoshina-Ishii, T. Asefa, M. J. MacLachlan, N. Coombs, G. A. Ozin, *Chem. Commun.* **1999**, 2539.
- [16] S. Guan, S. Inagaki, T. Ohsuna, O. Terasaki, *J. Am. Chem. Soc.* **2000**, 122, 5660.
- [17] T. Asefa, C. Yoshina-Ishii, M. J. MacLachlan, G. A. Ozin, *J. Mater. Chem.* **2000**, 10, 1751.
- [18] Y. Lu, H. Fang, N. Doke, D. A. Loy, R. A. Assink, D. A. LaVan, C. J. Brinker, *J. Am. Chem. Soc.* **2000**, 122, 5258.
- [19] M. McInall, J. Scott, L. Mercier, P. J. Kooyman, *Chem. Commun.* **2001**, 2282.
- [20] L. Mercier, T. J. Pinnavaia, *Chem. Mater.* **2000**, 12, 188.
- [21] H.-J. Im, Y. Yang, L. R. Allain, C. E. Barnes, S. Dai, Z. Xue, *Environ. Sci. Technol.* **2000**, 34, 2209.
- [22] A. Bibby, L. Mercier, *Chem. Mater.* **2002**, 14, 1591.
- [23] J. C. P. Broekhoff, J. H. de Boer, *J. Catal.* **1968**, 10, 377.

[\*] Dr. R. Adelung, Prof. F. Ernst  
Department of Material Science and Engineering  
Case Western Reserve University  
10900 Euclid Ave., Cleveland OH 44106 (USA)  
E-mail: rxa57@pop.cwru.edu

A. Scott, Prof. M. Tabib-Azar  
Department of Electrical Engineering and Computer Science  
Case Western Reserve University  
10900 Euclid Ave., Cleveland OH 44106 (USA)

Dr. L. Kipp, Prof. M. Skibowski  
Institut für Experimentelle und Angewandte Physik  
Christian Albrechts Universität zu Kiel  
Leibnizstr. 19, D-24098 Kiel (Germany)

S. Hollensteiner, Dr. E. Spiecker, Prof. W. Jäger  
Center for Microanalysis  
Technische Fakultät der Christian Albrechts Universität zu Kiel  
Kaiserstr. 2, D-24143 Kiel (Germany)

Dr. S. Gunst, Dr. A. Klein, Prof. W. Jägermann  
Fachgebiet Oberflächenforschung, Fachbereich Materialwissenschaften  
Technische Universität Darmstadt  
Petersenstr. 23, D-64287 Darmstadt (Germany)

Dr. V. Zaporozhchenko, Prof. F. Faupel  
Lehrstuhl für Materialverbunde  
Technische Fakultät der Christian Albrechts Universität zu Kiel  
Kaiserstr. 2, D-24143 Kiel (Germany)

[\*\*] RA gratefully acknowledges a grant by the Alexander von Humboldt foundation. Work was supported in part by the Deutsche Forschungsgemeinschaft, especially Forschergruppe DE 412/21 and project contract JA 908/4-1/4; the Wright Patterson Air Force base, the NSF and NIST. Equipment was provided by Prof. G. Chottiner.

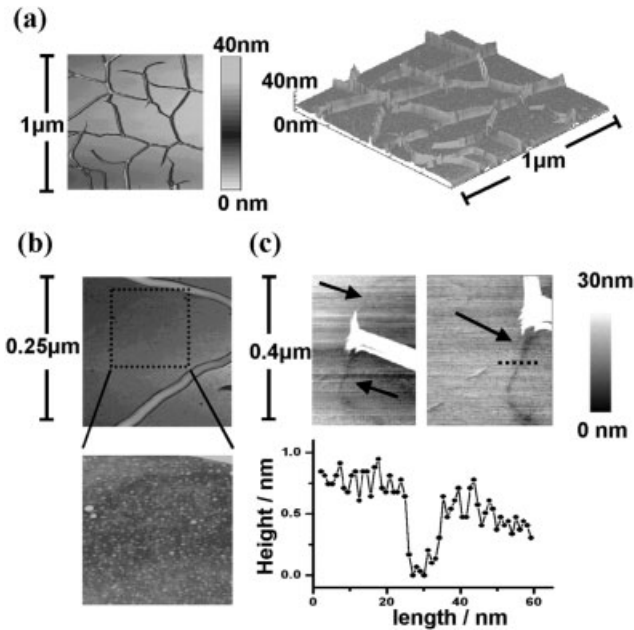


Fig. 1. STM images of copper-induced nanowires after the adsorption of an equivalent of approx. 2.7 monolayers of copper. a) Left: planar view, right: 3D representation. b) Clusters between the wires (enlarged section of a). c) End of a nanowire, which is just about to split up. The darkest features (arrowed) are cracks, a line scan along the dotted line shows the depth profile of the crack.

more or less regular network. Between the nanowires, we observe nanoclusters (Fig. 1b). However, the height of these clusters is more than an order of magnitude lower than the smallest wires. Even with the cluster coverage the crystal still exhibits a pronounced flat surface.

In Figure 1, the nanowires appear to have a diameter of about 20 nm; however, STM tends to overrate the true diameter (see below). The meshes of the network have a typical mesh diameter of 200 nm. Wires that are not connected to other wires at both ends are observed to terminate in sharp tips. Moreover, on terminating the nanowire growth process at an early stage (Fig. 1c), we observe cracks in the layered-crystal substrate, partly filled with nanowires. The depth of the cracks corresponds to the thickness of the topmost triple-layer of the substrate. In many instances, the cracks in the substrate are filled with nanowire up to right before the crack tip. As a consequence, the loose end of a wire appears as a tip, as mentioned before. Examples of these features can be found in Figure 1c.

Although grown in UHV, the nanowire networks we obtain by depositing Cu onto VSe<sub>2</sub> are remarkably stable under ambient conditions. Figure 2 presents images we have obtained by scanning electron microscopy (SEM) after exposing the material to air for about one month. Nevertheless, the images exhibit the same typical topography as the STM images of Figure 1, which were recorded immediately after the growth process. Besides a few contamination spots (Fig. 2b and arrows in Fig. 2a), which appear as dark features, no change in the appearance of the nanowire network can be observed. This proves that the nanowire networks are stable under ambient conditions, including atmospheric air pressure and

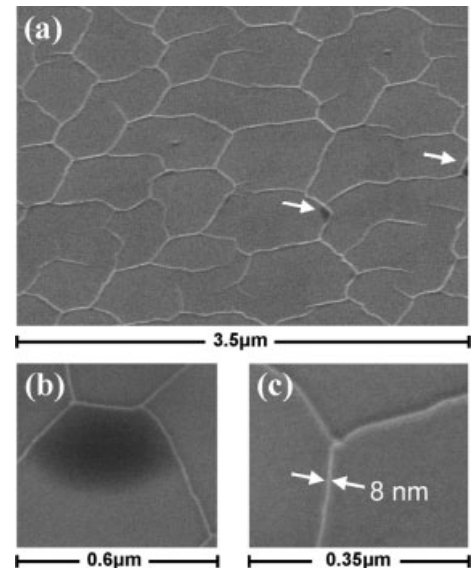


Fig. 2. SEM images of the copper-induced nanowires. a) Overview recorded at specimen tilt of 45°. b) Organic contamination (dark region) bound by nanowires. c) High-resolution image showing the true width of a nanowire.

humidity, which renders them robust enough for a variety of potential applications.

The nature of the contamination spots in Figure 2 remains uncertain, as energy dispersive X-ray spectroscopy (EDX) (in the scanning electron microscope) did not indicate any change in the chemical composition at the corresponding locations. Therefore, and from the fact that no contamination spots have been observed in STM, we conclude that the corresponding material was deposited only after the specimen was exposed to air. Note that the lateral extension of the contaminated regions is controlled by the nanowires, as if the nanowires represented a “nano-dam” for the contaminants.

While Figures 1 and 2 basically reveal the same information, the resolving powers of STM and SEM are somewhat complementary. STM has an excellent depth resolution, however the lateral resolution is limited by the lateral extension (“sharpness”) of the scanning tip. The field-emission scanning electron microscope we employed for obtaining the images in Figure 2, in contrast, provides more realistic information on the lateral dimensions of the nanowires but has comparatively poor depth resolution.

Combining the information from both techniques, we conclude that nanowires are approximately equiaxed (thus, they are as high as they are wide). The diameter of the nanowires can be as small as 8 nm, which corresponds to less than ~25 interatomic spacings, and wires with this small a diameter can extend over a length of several micrometers (Fig. 2c).

To understand the growth mechanism of the nanowires, we devised two experiments to disturb the homogeneous growth of the nanowire networks in a controlled manner. In the first experiment, we introduced a step in the substrate. As mentioned before, cleaving a layered-crystal usually generates perfectly flat surfaces. However, by cleaving the crystal under an angle, with the help of a shear force, one can generate surface

steps. This leads to inhomogeneous growth (Fig. 3a). Especially in the step-edge regions, nanotunnels or buckles appear. The diameter of these features can be as small as 50 nm (Fig. 3b).

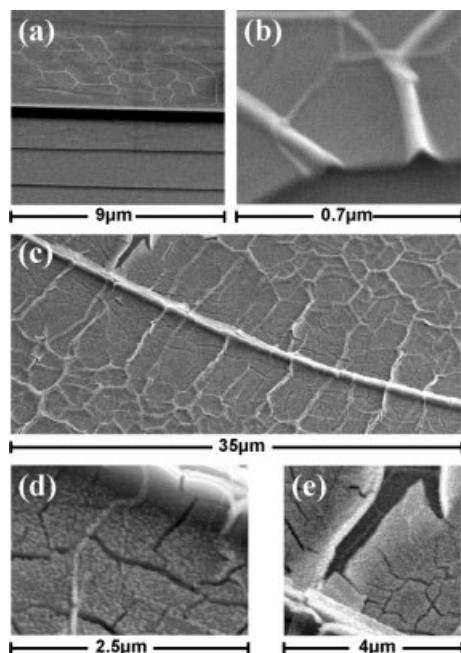


Fig. 3. SEM images (recorded at specimen tilt of 45°) revealing inhomogeneous coverage of the substrate with nanowires on a terrace. a) Nanowire networks on a terrace. b) Nanotunnels at a step edge. c) Substrate fold surrounded by nanowires, obtained after depositing a large amount of copper. d) Magnified selection of (c) showing cracks, folds, and nanowires. e) Destroyed nanowire network and formation of a nanowire network on the freshly exposed layer below.

In the second experiment, to learn more about the growth mechanisms of the nanowires, we changed the evaporation conditions. Figures 3c–e show a sample that was exposed to a large amount of copper (~50 monolayers). The sample contains some large buckles with a typical separation of 50 μm. At the same time, buckling of the sample as well as cracks can be found. At first sight, this is surprising, since buckling originates from compression, while cracks of the type observed here open under tensile stresses.

In Figure 3d, the sample surface seems to be covered by an almost continuous film instead of the single clusters observed in Figure 1. Despite the thick coverage, however, individual wires are still visible. Some surface areas are bent upwards (Fig. 3e), so that they expose the underlying material. The magnified image shows that a new nanowire network starts to form at the surface under the parts that are bent away. This observation suggests that the entire layered-crystal can be disassembled triple-layer by triple-layer by depositing a suitable big amount of Cu leading to nanowire networks, buckling, and cracks.

Since the Cu-induced nanowires withstand air exposure at room temperature, they can be studied by a great variety of characterization methods. For example, they can be analyzed by light optical microscopy. Owing to their nanoscopic dimensions, it is of course not possible to resolve two closely spaced nanowires under the usual imaging conditions of this tech-

nique, however, individual nanowires still give a line of contrast. Under certain evaporation conditions the separation of the nanowires remains larger than the wavelengths of visible light, and then individual wires can actually be imaged by light optical microscopy. Figure 4 shows a region close to the edge of a nanowire sample. Near the edge, the image indicates parallel wires along the direction normal to the edge. Some 10 μm away from the edge, these wires form a nanowire network with the usual appearance.

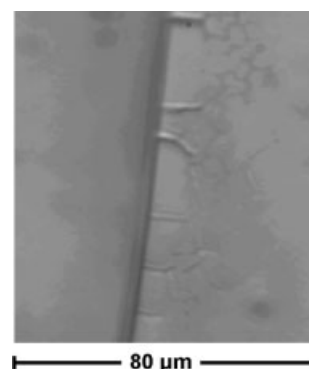


Fig. 4. Optical micrograph of a crystal edge with copper-induced nanostructure.

A second tactile technique we have applied to study the Cu-induced nanowire networks is atomic force microscopy (AFM), which can be performed in air. In non-contact mode in air, AFM reveals the same topography of the nanowire networks as STM and SEM. Figure 5a presents an overview AFM image, covering a region of 6 × 6 μm. Despite the lim-

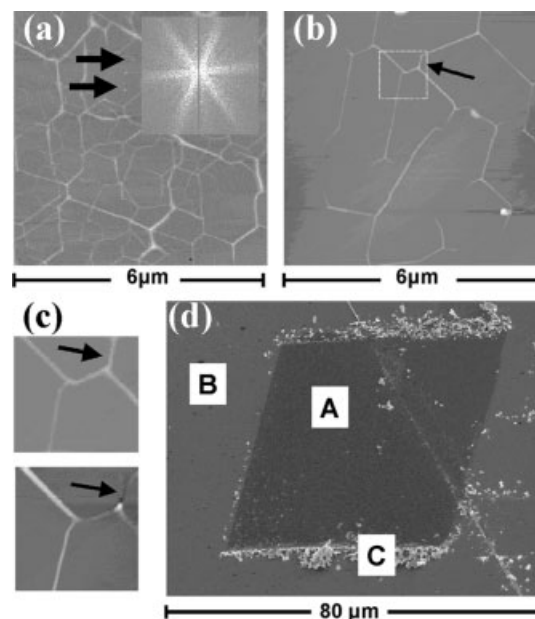


Fig. 5. AFM images and manipulation of nanowire networks. a) Contact mode overview. Inset: power spectrum of the image. Arrows point to some bigger clusters. b) Contact mode image showing a less dense network. c) Magnified network segment of (b) before and after manipulation with the AFM tip (arrows in b,c). d) nanowire removed from a 50 × 50 μm<sup>2</sup> area, recorded at specimen tilt of 45°. Region A: removed nanowires, region B: nanowires are still intact, and region C: removed nanowires pile up in wells of debris.

ited resolution of AFM in air compared to STM in UHV, the AFM image also reveals some of the bigger Cu clusters between the nanowires (arrows). The inset shows the power spectrum of the image, obtained by fast Fourier transform. The power spectrum reveals features with a six-fold symmetry, which indicates a preferential alignment of the nanowires.<sup>[2]</sup>

AFM images recorded in contact mode appear similar to those recorded in the non-contact mode, which indicates that the nanowires can withstand the relatively large forces exerted on them in contact mode. To increase the mechanical load on the nanowires, we set the feedback to the strongest available down force. In combination with the fastest scan speed available on the instrument,  $100 \mu\text{m s}^{-1}$ , we applied the maximum attainable lateral force on the nanowires. Even during this treatment no destruction of the nanowires was observed. Also, scanning 10 times with high speed over the same surface area has no destructive effect on the nanowires. The pronounced resistance of the nanowires against plastic deformation is enabling a variety of experiments that require mechanical contact, such as measurements of the electrical conductivity. The high mechanical strength of the nanowires is also beneficial for applications with material combinations, for example nanowires and molecules.

The advantage of self-assembled nanostructures lies in the large amount of structures that one can produce in a short time. The disadvantage is that the morphology of these structures is often difficult to control or design. For the nanowire networks we consider here, however, this deficiency can be overcome as follows. Figures 5b and c show that it is possible to re-arrange parts of the network to a desired circuit of wires by disconnecting distinct wires. The method we discovered here is to scan over the area in which the wires should be removed for many times (about 50 times within 2 h) in contact mode. Once a part of a wire is disconnected, it is quick to completely remove it. Note that this operation exposes a one triple-layer deep crack.

By means of EDX in a scanning electron microscope, we analyzed the composition of the surface region exposed by removing the Cu nanowire network in a  $50 \times 50 \mu\text{m}^2$  by contact-mode AFM. EDX was also carried out in the adjacent regions, where the nanowires were still intact, and at the side of the scanned area, where the material of the removed nanostructures piles up in wells of debris (Fig. 5d). In the region where the nanowires were removed, EDX did not indicate any measurable concentration of Cu. In regions where the nanostructures were still intact, in contrast, a Cu signal was detected. In the debris wells, we obtained a pronounced strong Cu signal. Moreover, oxygen was detected in the wells.

Transmission electron microscopy (TEM) of ion-milled plan view specimens has been employed to characterize the arrangements, structure, and dimensions of the nanostructures after deposition of copper onto the cleaved layered crystals of  $\text{VSe}_2$ . On the flat parts of the substrate, self-similar nanowire networks with wire diameters ranging from about 8 nm to about 250 nm and mesh dimensions ranging from  $0.35 \mu\text{m}$  up

to  $\leq 10 \mu\text{m}$  are observed. Additionally, nanoclusters are formed within the meshes of the nanowire networks. The nanowires are preferentially aligned along the close-packed  $\langle 1\bar{2}10 \rangle$  and  $\langle 10\bar{1}0 \rangle$  crystal directions (Fig. 6a). Nanowires of medium and large diameter show complex geometry with two

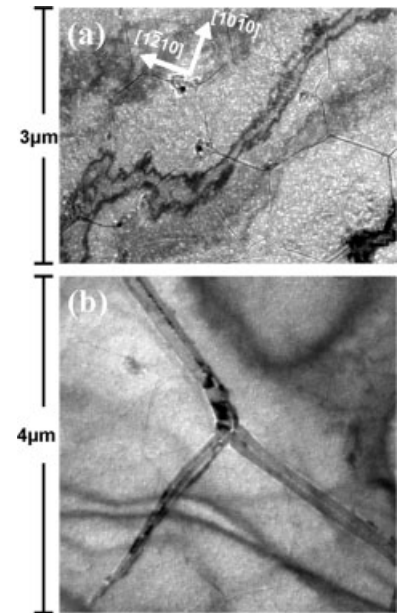


Fig. 6. TEM bright-field images of a plan view specimen. a) Small- and medium-size nanowire networks and nanoclusters. Nanowire orientations preferentially along  $\langle 1\bar{2}10 \rangle$  and  $\langle 10\bar{1}0 \rangle$ . b) Large-size nanostructures with complex geometry and polycrystalline structure.

separated wire strands. Whereas the wire segments of the networks show rather uniform lateral dimension, ending segments sharpen at their tip regions. Combined bright- and dark-field imaging and electron diffraction studies indicate that the wires are polycrystalline (Fig. 6b).

All experiments presented here were performed using  $\text{VSe}_2$  layered crystals as the substrate. However, preliminary SEM studies revealed that Cu also induces nanowire networks when deposited onto  $\text{TiSe}_2$  layered-crystals. We conclude, therefore, that the formation of nanowire networks by Cu deposition is a common phenomenon on layered-crystals.

In summary, the following conclusions can be drawn from the experimental results. Deposition of Cu onto the surface of a transition-metal dichalcogenide layered crystal induces self-assembly of several kinds of nanostructures: i) Nanotunnels form and can be observed at step edges of layered crystals cleaved by a shear force, ii) networks of cracks form within the topmost triple-layer of the substrate, and iii) networks of nanowires form in conjunction with cracks. These nanowire networks cover the entire substrate surface, which can have dimensions on the centimeter-scale. Depending on the fabrication conditions, nanowires with a diameter as small as 8 nm can be obtained.

Note that beside the clusters, which are more than an order of magnitude smaller in height than the lowest nanowires, the inside of the network meshes is perfectly flat. Therefore, the

Cu-induced nanowires are particularly accessible for several important analytical methods of materials science. Moreover, these structures show a remarkable mechanical strength and stability under ambient conditions. Therefore, they are also accessible with analytical techniques that do not need a UHV environment. Because of their mechanical strength, non-destructive combination of the nanowires with other materials appears to be possible. (Indeed, we are presently performing first successful experiments of attaching macromolecules to the nanowires by a wet chemical method.<sup>[3]</sup>)

In order to explain the formation of self-assembled nanowire networks by Cu deposition on layered crystals, we need to account for the observation that both cracks and buckling were observed at the substrate surface, thus signs of both dilative and compressive stresses. These experiments suggest that the growth of the nanowires is induced by a change in the lattice parameter of the first layer. It is known<sup>[4]</sup> that metal atoms adsorbed on transition-metal dichalcogenide layered-crystal surfaces donate their outer electrons to the substrate crystal. Acceptance and delocalization of these electrons by the substrate crystal cause compressive stresses, which tend to expand the lattice parameter.<sup>[5,6]</sup> In order to release the compressive stresses, in extreme cases buckles form in the uppermost triple-layer. At a later stage, the concentration of Cu atoms on the substrate surface becomes large enough to induce the formation of Cu clusters. Consequently, the electrons donated to the substrate in the beginning are withdrawn and localized near the clustering copper atoms. As a result, dilative stresses evolve, which tend to shrink the lattice parameter of the topmost triple-layer. Consequently, the topmost triple-layer fails by cracking. Since the dilative stresses are homogeneous, a more or less regular crack pattern evolves—similar to the crack pattern usually observed in dried mud.

At first sight it appears contradictory that both buckles and cracks appear side by side on the same surface. This can be explained, however, by the observation<sup>[7]</sup> that the crystal will not only expand when accepting electrons from deposited Cu atoms, but will also become mechanically weaker. Besides the Cu clusters, the opening cracks act as further (and much more efficient) condensation points for Cu atoms. Condensation of Cu atoms in opening cracks, however, withdraws more electrons from the topmost triple-layer, which promotes further dilative stresses and, consequently, further cracking. At the end of this process, most of the deposited single Cu atoms are incorporated in nanowires, while a minor fraction remains agglomerated in Cu clusters between the wires. This model explains all experimental observations presented here as well as the behavior of Rb found in our earlier studies.<sup>[1,8]</sup> In particular, it explains that loose ends of nanowires always appear tipped in STM images and end shortly before the tip of the crack in which they are embedded. It is obvious, however, that more measurements have to be performed to confirm the details of the model we propose here, which extends the model proposed before.<sup>[8]</sup>

From light optical microscopy it is evident that different, aligned nanostructures form at the sample edge. In wet chemi-

cal intercalation experiments a similar phenomenon occurs.<sup>[9]</sup> In the wet chemical intercalation process metal ions from an electrolyte are intercalated in a layered crystal by applying an external voltage. According to previously published results,<sup>[9]</sup> an intercalation of atoms occurs to a finite penetration depth from the edges of the crystal. The nanostructures observed in Figure 4 may have the same origin, if intercalation also takes place in UHV, as suggested in the literature.<sup>[6,10,11]</sup>

Irrespective of the details concerning the formation process, the nanostructures described here are very useful for nanostructure research. They form in a simple process and possess high mechanical strength and a significant elevation over a flat surface. These features render Cu-induced nanowire networks particularly accessible to many powerful techniques of micro-characterization, electrical characterization, mechanical experiments, and to emerging techniques of combining different objects of the nanoworld with each other.

## Experimental

The single-crystalline VSe<sub>2</sub> layered-crystal substrates we employed were grown by a CVT (chemical vapor transport) process, which has been in use for more than 30 years [12]. Foil-like single crystals up to several square centimeters in size are obtained in this way. The surface of these crystals appears flat and shiny. The macroscopic appearance reflects the atomic structure of this material. Layered-crystals consist of coherently stacked triple-layers with the sequence ...X-T-X|X-T-X|X-T-X..., where T denotes a monolayer of a transition metal (V, Ti, etc.) and X a monolayer of another element (Se, S, etc.) [13], a chalcogen atom. In both type of monolayers (X and T) the atoms are arranged on a hexagonal lattice with the same lattice parameter. While strong covalent and ionic forces act within each triple layer X-T-X, only weak (van der Waals) forces act across the boundaries between neighboring triple layers. This enables the crystal to cleave easily between the triple layers, and the surfaces exposed by cleaving are known as high-structural-quality substrates for deposition experiments in UHV. For such experiments, the layered crystals can either be cleaved directly in the UHV or under ambient conditions before loading. In the latter case, subsequent heating in UHV to 110 °C is known to produce a clean surface. Layered-crystal substrates prepared in this way often possess a surface that is atomically flat over hundreds of square micrometers without any structural defects.

In the experiments reported here, we used a thermal Cu evaporator (a tungsten filament with a Cu wire attached to it). Feeding an electric current of 3 to 6 A typically leads to Cu partial pressures of 10<sup>-9</sup> to 10<sup>-7</sup> mbar. In order to perform the Cu deposition in a well-controllable manner, we chose the distance between the sample and the Cu source such that the amount of Cu deposited after three minutes corresponded to a few monolayers (depending on the distance, we usually obtained around three monolayers).

STM was carried out using a modified OMICRON MICRO STM with additional high-efficiency eddy-current damping system. Tunneling currents used were 200 pA. SEM was done using a Hitachi high-resolution SEM. An Omnimet video microscope was used for optical microscopy. AFM was performed on Parc Scientific Instruments Autoprobe AFM and Thermomicroscopes Explorer AFM instruments. TEM images were obtained using a Phillips CM 30 transmission electron microscope.

Received: February 13, 2002

Final version: April 24, 2002

- [1] a) R. Adelung, L. Kipp, J. Brandt, L. Tarcak, M. Traving, C. Kreis, M. Skibowski, *Appl. Phys. Lett.* **1999**, *74*, 3053. b) R. Adelung, J. Brandt, K. Rossnagel, O. Seifarth, L. Kipp, M. Skibowski, C. Ramirez, T. Strasser, W. Schattke, *Phys. Rev. Lett.* **2001**, *68*, 1303.
- [2] A preferential alignment was also observed in the case of Rb nanowire networks [1].
- [3] R. Adelung, A. Scott, F. Ernst, L. Kipp, M. Skibowski, M. Tabib-Azar, paper presented at *The Ninth Foresight Conference on Molecular Nanotechnology*, Santa Clara, CA, November 9–11, **2001**.

- [4] C. A. Papageorgopoulos, M. Karamatos, A. Papageorgopoulos, A. Schellenberger, E. Holub-Krappe, C. Pettenkofer, W. Jaegermann, *Surf. Sci.* **1995**, 275, 314.
- [5] C. Ramirez, W. Schattke, *Surf. Sci.* **2001**, 482–485, 424.
- [6] H. I. Starnberg, H. E. Brauer, L. J. Holleboom, H. P. Hughes, *Phys. Rev. Lett.* **1993**, 70, 3111.
- [7] A. Rettenberger, P. Bruker, M. Metzler, F. Mugele, T. W. Matthes, M. Böhmisch, J. Boneberg, K. Friemelt, P. Leiderer, *Surf. Sci.* **1998**, 402–404, 409.
- [8] R. Adelung, J. Brandt, L. Kipp, M. Skibowski, *Phys. Rev. B* **2001**, 63, 165 327.
- [9] a) J. Heitmann, J. McCallum, W. Tröger, T. Butz, *Nucl. Instr. Meth. Phys. Res. B* **1999**, 158, 689. b) J. Heitmann, J. McCallum, W. Tröger, T. Butz, *Nucl. Instr. Meth. Phys. Res. B* **2000**, 161, 619.
- [10] C. Pettenkofer, W. Jaegermann, *Phys. Rev. B* **1994**, 50, 8816.
- [11] I. Ekvall, H. E. Brauer, E. Wahlstrom, H. Olin, *Phys. Rev. B* **1999**, 59, 7751.
- [12] H. Schafer, *Chemical Transport Reactions*, Academic Press, New York **1964**.
- [13] F. Levy, *Crystallography and Crystal Chemistry of Materials with Layered Structures*, Reidel, Dordrecht, The Netherlands **1968**.

## Polyfluorenes with Dendron Side Chains as the Active Materials for Polymer Light-Emitting Devices\*\*

By Alexander Pogantsch, Franz P. Wenzl, Emil J. W. List,\* Günther Leising, Andrew C. Grimsdale, and Klaus Müllen

The last decade has witnessed intense research on conjugated polymers as promising materials for optoelectronic applications. While initially poly(*p*-phenylenevinylenes) (PPVs),<sup>[1]</sup> poly(*p*-phenylenes) (PPPs),<sup>[2]</sup> and polythiophenes (PTs)<sup>[3]</sup> were in the focus of investigation, in the last years polyfluorenes (PFs)<sup>[4]</sup> have emerged as a further important member of the family of conjugated polymers.

PF homopolymers show strong blue fluorescence emission, so that they can be applied as active layers in polymer light-emitting devices (PLEDs)<sup>[5]</sup> and as host material for internal color conversion techniques.<sup>[6]</sup> Various PF copolymers were synthesized with emission colors covering the entire visible spectrum<sup>[7,8]</sup> and the liquid crystalline nature of most of the PFs allows for specific orientations and thereby enables the realization of PLEDs generating polarized light emission.<sup>[9]</sup>

One drawback of conjugated polymers in solid-state device applications is the quenching of luminescence by intermolecu-

lar interactions,<sup>[10]</sup> chemical defects,<sup>[11]</sup> and excited states such as polarons.<sup>[12,13]</sup> In order to reduce these quenching effects the use of dendrimers was suggested.<sup>[14]</sup> However, care has to be taken since a diminution of intermolecular interactions will on the downside reduce charge carrier transport. It is therefore necessary to use bulky side chains, such as dendronic side chains, that will not negatively influence charge transport but rather partake in the transport process while not contributing to the electroluminescence (EL) emission of the material. These building blocks are the first step for the development of functionalized electroactive polymers, in which the side groups possess both shielding and charge transport properties.

Using this materials concept, we have recently reported<sup>[15]</sup> the synthesis of a polyfluorene with polyphenylene (Müllen-type) dendrons as side chains and have shown that PLEDs prepared from these materials possess very promising properties. It was shown that the chemical stability and the shape persistence of Müllen-type dendrimers allows an effective shielding of the polyfluorene backbone at lower dendron generation numbers compared to Fréchet-type ones.<sup>[16]</sup>

However, we found from our previous results<sup>[15]</sup> that the benzyl linkage incorporated in the sidechain of the polymer that was used for the PLEDs is prone to photooxidation,<sup>[17]</sup> which has serious drawbacks for device stability. Therefore, we have synthesized a novel dendronic PF (DPF) possessing Müllen-type dendrons with a shortened and more stable linkage compared to the one previously reported, which will be discussed in the following.

The molecular structure of the discussed polymer is depicted in the inset of Figure 1, the material has a high glass-transition temperature of about 250 °C, which is a requisite for high-stability applications in optoelectronic devices, and does not show a liquid crystalline phase. Solid-state optical spectra and those in dilute dichloromethane solution are shown in Figure 1. We find that the ground-state absorption

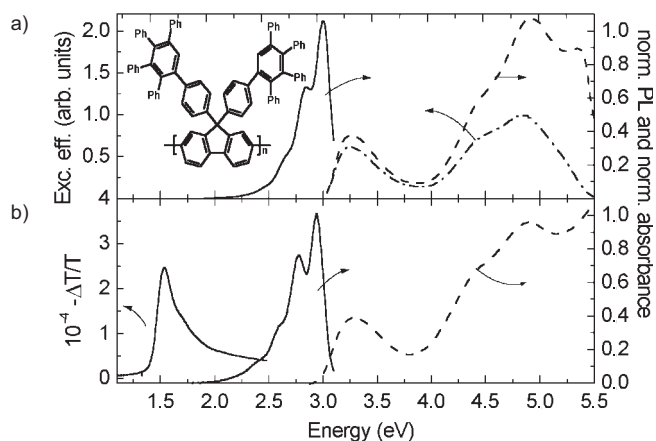


Fig. 1. a) PL spectrum (solid line), optical density (dashed line), excitation efficiency (dash-dotted line) of a dilute solution of a DPF. The inset shows the chemical structure of DPF (Ph stands for a phenyl ring). b) PL spectrum (solid line, right axis), PA spectrum (solid line, left axis), and optical density (dashed line) of a thin solid film of DPF.

[\*] Dr. E. J. W. List,<sup>[+]</sup> A. Pogantsch, F. P. Wenzl  
Christian Doppler Laboratory for Advanced Functional Materials  
Institute of Solid State Physics, Graz University of Technology  
Petersgasse 16, A-8010 Graz (Austria)  
E-mail: e.list@tugraz.at  
Prof. G. Leising<sup>[+]</sup>  
Science & Technology AT&S AG  
Fabriksgasse 13, A-8700 Leoben (Austria)  
Dr. A. C. Grimsdale, Prof. K. Müllen  
Max-Planck-Institute for Polymer Research  
Ackermannweg 10, D-55128 Mainz (Germany)

[+] Second address: Institute of Nanostructured Materials and Photonics, Joanneum Research Inc., Franz-Pichler-Strasse 30, A-8160 Weiz, Austria.

[\*\*] We gratefully acknowledge the financial support by the SFB "Elektroaktive Stoffe" and WVF project P14170-TPH.